Nonlinear Dyn (2018) 91:1791–1816
https://doi.org/10.1007/s11071-017-3981-4

ORIGINAL PAPER

Development and validation of a numerical model for the simulation of high-velocity impacts on advanced composite armor systems

Giovanni Sabadin · Marco Gaiotti · Cesare M. Rizzo · Alessio Bassano

Received: 29 March 2017 / Accepted: 29 November 2017 / Published online: 7 December 2017

Abstract The anti-ballistic properties of a new advanced composite armor system have been investigated with the aim to minimize the armor system total weight per unit area. The innovative protection, made of a silicon carbide ceramic outer layer and an inner composite back-packing layer formed by ultra-high molecular weight polyethylene (UHMWPE) fibers, namely Dyneema® Hard Ballistic 26, was realized and then tested performing dedicated ballistic impact tests. In order to investigate its permanent deformation, ceramic cracking, dimension of the rupture, and extension of the impact damage, nondestructive and destructive tests were conducted on the tested panels. The experimental results were used to develop and validate a transient nonlinear dynamic simulation model of the high-velocity impact of a 7.62 AP bullet on the tested armor system. After an accurate setting of the parameters involved in the description of the material constitutive models and of the involved physical phenomena, a complex numerical model was developed in the ANSYS-Autodyn® environment using both mesh and meshless approaches at the same time. The comparison reveals a good agreement between experimental and computational results in terms of ballistic properties, deformations, fragmentation, and fracture of the ballistic armor system. Hence, a new numerical model for the design and the optimization of the ballistic efficiency of composite armor systems was developed and can be now used in current practice.

Keywords High-velocity impact · Composite · Multilayer · Armor system · Ballistic tests · Numerical simulation

G. Sabadin · M. Gaiotti (✉) · C. M. Rizzo
Marine Structures Testing Lab, DITEN, University of Genova, Via Montallegro 1, 16145 Genoa, Italy
e-mail: marco.gaiotti@unige.it

G. Sabadin
e-mail: giovanni.sabadin@gmail.com

C. M. Rizzo
e-mail: cesare.rizzo@unige.it

A. Bassano
OTO Melara a Finmeccanica company, Via Valdilocchi 15, 19136 La Spezia, Italy

1 Introduction

The application of advanced composite materials in the development of armor systems is well established. Compositions of novel materials are particularly suitable for the integration and improvement of ballistic protections in key sectors of the defense industry, especially in the automotive, aeronautical and, more recently, in the shipbuilding industry. The significant reduction in the total armor weight obtained by the use of these new materials in lieu of traditionally hard steel protections made by rolled homogeneous armor steel (RHA) is well known [6]. The reduction in total armor weight generally leads to an increase in the vehicle performance in terms of speed and maneuverability: This means the improvement of the survivability of the vehi-

Table 1 Values of the density ρ, tensile failure strength σ_f and the failure strain ε_f measured at the strain rate $\dot{\boldsymbol{\varepsilon}}$ and the corresponding value of the Cunniff velocity C*(Reproduced with permission from Russell et al. [26])

FIBER	ρ (kg m^{-3})	$\dot{\boldsymbol{\varepsilon}}$ (s^{-1})	σ_f (GPa)	ε_f(%)	C^* (ms^{-1})
Dyneema®	970	700	2.55	6.26	698
Spectra 900	970	433	2.5	3	689
M5	1700	Not stated	4	1.4	712
Toray T1000	1800	Not stated	6.4	2.2	947
Toray T700	1570	1000	3.4	1.57	665
Kevalr 49	1440	1350	3.08	3.86	650

cle and the protection of the crew members in a combat situation.

Actually, the new advanced composite armors (ACA) are built up by different multilayers of materials in order to guarantee the ballistic protection at different levels of threats as described, e.g., in standards like the NATO-STANAG–4569 [23] or the U.S. NIJ Standard 0108.01 [22]. For relatively weak threats, a suitable number of single layers of fiber-reinforced polymer–matrix composite is sufficient, see, e.g., [10,21]. When increasing the threats, it becomes necessary to develop a combination of different materials in order to guarantee the ballistic protection [7,25]. Nowadays, best innovative solutions and lighter armor systems are made up of an outer layer of ceramic materials and a back-packing in fiber-reinforced polymer–matrix. In fact, the ability of a composite armor to provide useful contribution to an impact event depends on the hardness of the ceramic materials, which is critical for blunting and eroding the projectile, and the strain to failure of the fiber reinforcement, which determines the ability of those materials to absorb kinetic energy via a global deformation process. Different ceramic materials can be adopted in the form of ceramic tiles in the protections such as alumina (Al_2O_3), silicon carbide (SiC), or boron carbide (BC): density and properties of the ceramic vary proportionally to their cost. Only when an extremely low weight is required, expensive SiC and BC tiles are used.

For the back-packing layers, different innovative fibers can be applied such as polypropylene fibers (e.g., Tegirs®), aramidic fibers widely known as Kevlar® and, more recently, a new composite material made of ultra-high molecular weight polyethylene (UHWMPE) fibers, very suitable to absorb the energy of a ballistic impact. These innovative fibers, commercialized in the late 1970 under the trade name Dyneema®, have densities less than water (0.97 kg/m^3) and high tensile ultimate stress, in excess of 3 GPa [18]. Their very high specific strength and stiffness led to their use in many different fields, e.g., high-performance sails, fishing lines and marine mooring cables; woven fabrics are used to make protective gloves.

Since the initial numerical study on the ballistic performances of laminates reinforced by UHMWPE fiber as reported by Frissen [9], it was noted that the mechanical properties are competitive for ballistic and blast applications. Nowadays, it is well known that the hard ballistic Dyneema® guarantee excellent protection against threats and fast-moving improvised explosive device (IED) fragments. As reported in Russel et al. [26], and namely from the value of the mechanical properties reported in Table 1, it is clear that UHWMPE fibers are very competitive for ballistic and blast application. Cunniff defined the velocity C* [4] that express the ballistic performance of the fibers in terms of maximum bullet velocity. At the same time, the UHWMPE density is considerably lower with respect the other fibers having similar ballistic performances, not to mention metallic materials. Published data on Dyneema® are very scattered and the first characterization of the dynamic behavior of a Dyneema® composite is rather recent in relevant literature, see [10,16]. Only in recent years, the research focused extensively on the description of the dynamic behavior and properties of such materials in order to extend material models to armor-grade composite materials. The main contributes derive from the research of Russel et al. [26], Karthikeyan et al. [18], and Lässig et al. [20]. Very recent research focuses on the penetration mechanism of a steel sphere onto composite armor systems made by Dyneema® Hard

Ballistic 26 as presented in O'Masta et al. [24]. The definition of a high-fidelity material model moves the challenge in the dynamic numerical simulation of the high-velocity impact (HVI) of the bullet into the advanced composite target using dynamic phenomena simulation software, e.g., Ls-Dyna®, Abaqus® or ANSYS-Autodyn®. Indeed, the possibility of properly simulating the bullet impact onto a composite armor system is very useful to optimize layers' types and thickness and consequently to minimize the total weight of the protection without the need of rather expensive and complex experimental tests.

The lack in the literature of research focused on the impact simulation of 7.62 AP bullet on a composite armor system made of a ceramic layer and a back-packing of UHMWPE fiber-reinforced laminate moves the present study. In order to obtain a reliable numerical model, an intensive study was carried out comparing the experimental results of ballistic impact tests with the numerical results derived from simulations developed in the frame of a research project cooperation. The developed anti-ballistic solution applies advanced materials with high technological content and the most recent techniques for lamination and bonding. The created panel is a real innovation in the field of vehicle ballistic protection and even more in the defense systems, leading to significant savings in terms of total weight of the protection.

The request to develop and validate an innovative numerical model to simulate the impact of a bullet upon an add-on composite armor system was the challenge of the research involving the Italian company OTO Melara and DITEN of the University of Genova. The model was intended for patrol boats, finally aimed at minimizing total weight of the armor system but still securing a specific protection level and additionally withstanding the harsh marine environment. To guarantee the maximum reduction of the add-on protection weight, remarkable importance was paid to the application of innovative anti-ballistic materials and to their cost. After a first literature review and taking advantage of the know-how of OTO Melara, it was eventually decided to develop a new armor system made by a first layer of SiC ceramic glued onto a back-packing made of UHWMPE laminate.

Next, the initial development and validation of a numerical model of the projectile penetration into a target armor system [28], it was decided to improve and validate a new numerical model that allows obtaining impact behavior of a ballistic protection made of SiC ceramic and UHWMPE fibers. Due to the lack of experimental and numerical results in the literature concerning this impact typology, actually needed for a comparison with further numerical results, it was necessary to plan the realization of the add-on panels and the execution of dedicated ballistic test in order to obtain experimental results for model validation. After conducting the experimental campaign and evaluating the anti-ballistic capacity of the new armor system, an enhanced numerical model was developed through the implementation of "hydrocodes," i.e., software particularly suited to model HVI, bullet penetration and blast events, simulating the three-dimensional configuration of the bullet impacting upon the panels.

In the present paper, a complete description of the test cases as concern geometry, adopted material, construction method, and final dimension of the armor system is presented at first. Then, the required standard threat levels and the conducted ballistic impact tests are described. The destructive and nondestructive tests on the impacted specimens, including analysis of images of the damage and dimensions of the fracture for the different materials, are thereafter discussed. The definition of the numerical model, the calibration of the main parameters of the simulation software, and the related investigations about the physics of the phenomena are subsequently reported, particularly referring to the dynamic characterization of the material constitutive models for the UHMWPE fibers. Finally, comprehensive comparisons between the numerical simulation results and the experimental impact tests ones are reported, eventually validating the numerical model. Appositely hidden results are reported due to obvious confidentiality reasons.

2 Tests description

2.1 Armor system

For the ballistic impact tests, a rectangular add-on panel system has been realized in order to guarantee the fourth protection level (named Armor-Piercing Rifle) as defined by the NIJ Standard 0108.01 [22]. Here, the level of threat considered is a 30-06 M2 Armor Piercing (AP) bullet. Figure 1 shows one of the tested specimens.

The panels have square shape; they consist of a first outer layer made of ceramic tiles with high strength and hardness properties and a second back-packing layer

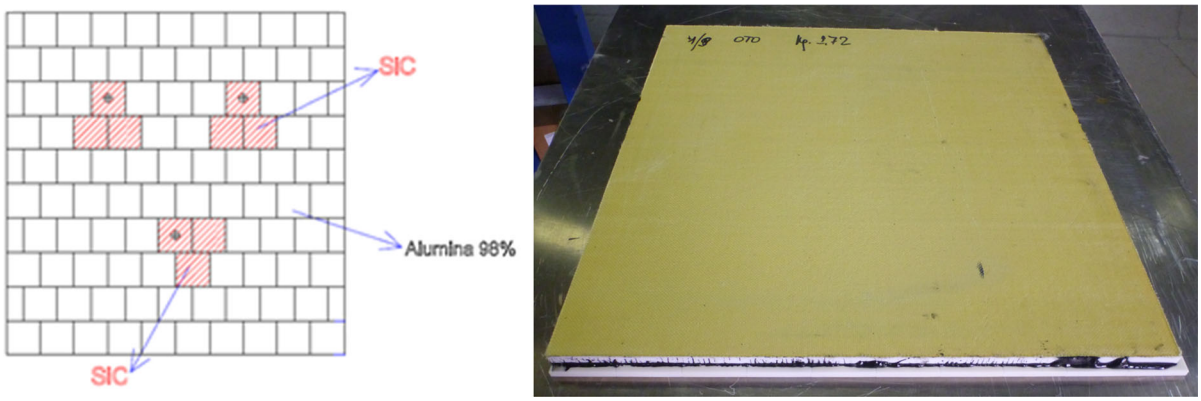

Fig. 1 Geometry of the tested panels

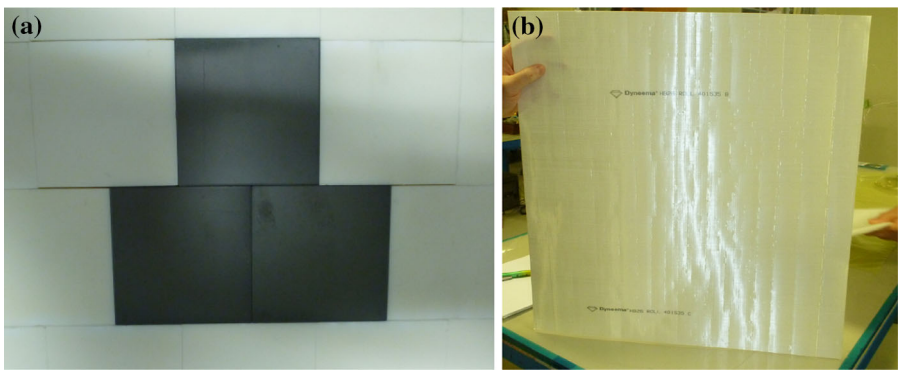

Fig. 2 Materials used in the panel: **a** tiles of silicon carbide; **b** single layer of Dyneema® hard ballistic 26

made of high modulus fiber composite; each layer is bonded to the other by a glue specifically produced for these assemblies. Each specimen was made to ensure the possibility of carrying three different impacts of a projectile in three distinct areas: The ceramic tiles material are positioned as shown in Fig. 1. Only nine tiles in the specimens were made by the rather expensive ceramic material selected for the composite armor system while cheaper Alumina 98% tiles were used for the remaining of the panel as usual in similar cases. In particular, the armor ceramic tiles used in all the tested panels as shown in Fig. 1 are silicon carbide (with a relatively low density of 3.15 g/cm^3 and a very high elastic modulus of about 410 GPa). The back-packings are made by an UHMWPE Dyneema® Hard Ballistic 26; these fibers are characterized by higher impact and fatigue strength compared to other ballistic materials as shown in Table 1. See Fig. 2.

Impacts are aimed at the SiC tile center, thus ensuring ballistics impacts comparable with those made by numerical simulation.

Each individual fabric layer has an areal density ranging between 257–271 g/m^2; for convenience, it is therefore considered an average density of the layers of 262 g/m^2, and each layer has an average thickness of 0.38 mm. The armor total thickness is less than 20 mm, but for confidentiality reasons this paper omits the actual thickness of the layers. These advanced materials allow containing the total areal density of the protection with respect to other anti-ballistic solutions commonly installed on land vehicles: In fact, the total areal density of the described add-on panel is 35 kg/m^2 approximately, while a value of about 40 kg/m^2 is the standard.

2.2 Cartridge 30-06 M2 SPRG description

The threats used for the ballistic tests are the cartridge caliber 30-06 M2 SPRG. This bullet is commonly called M2 Armor Piercing bullet and is identified by the black color on its front; also, the total length of the cartridge is 63.2 mm. The bullet inside the cartridge is composed by three different materials:

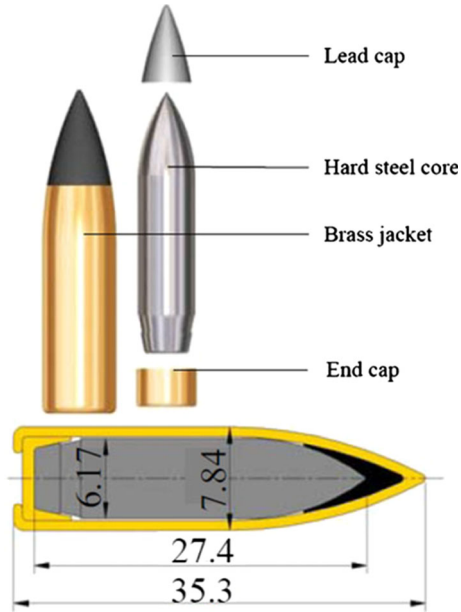

Fig. 3 30-06 M2 bullet from Forrestal et al. [8], measures in mm

an outer jacket made of cart brass, an internal core of hard steel, and the rear part in lead. The total weight of the bullet is 10.53 g, and the average total length is 35.3 mm. The dimensions shown in Fig. 3 represent the average size of the projectile of the cartridge in the manufacturing phase. Actually, these dimensions may have 0.01–0.02 mm deviations due to the manufacturing process.

The bullet is fired at an average speed of 868 m/s, thus constituting a significant threat in the field of projectiles having 7.62 caliber.

2.3 NIJ -0108.1 Standard and test set up

US NIJ Standard-0108.01 Ballistic Resistant Protective Materials establishes five degrees of threat based on caused damage and then provides the appropriate standard level of protection [22]. The standard was drafted to describe and share different types of configurations for bulletproof vests.

The protection level required in the frame of this research is the type IV (Armor-Piercing Rifle), where the reference ammunition for the qualification is the Armor Piercing 30-06 M2 with a total mass of 10.8 g and an impact velocity of 868 ± 15 m/s. This level of threat depicts the bullet impact used by sniper rifles against the target: the high internal energy of the projectile, its material properties and the geometry of the ogive make this ammunition the most lethal threat taken into consideration by the US Standard.

The technical specification indicates to hit each panel with three separate shots; each single shot must hit a single area of SiC tiles. The impact at the center of the tile will be useful to obtain an experimental comparison for the numerical simulations.

The ballistic tests are performed according to Fig. 4: Each panel is tested individually, repeating the operations for each of the three targets on the panel.

The test needs a few elements to be performed, besides many safety and security issues:

- A test manometric barrel is suitably supported to hit the targets in the selected points also analyzing temperatures and gases produced by the explosion.
- Between the barrel and the target, an optical barrier is placed allowing the precise and reliable determination of the speed of the projectiles, ranging from 500 to 1000 m/s. (An averaged value of 868 m/s was used in computations.)
- At a predetermined distance from the barrel, the target is placed on a support structure (Fig. 5), to constrain the panels. For these experimental tests, the panel is fixed only on the edges, leaving free the central part where the impact takes place.

3 Experimental results

3.1 Ballistic impact results

On each panel, three M2 bullets were fired in points marked in correspondence of the SiC tiles; see Fig. 6.

In Table 2 the results of the experimental tests are summarized: The panel protected by SiC tiles proved suitable to ensure the ballistic protection for the selected threat level.

Among nine impact tests performed on three panels, only one shot completely perforated the panel (CP, complete penetration), while the other eight shots were held by the armor. It was therefore decided to validate the full protection provided by the panel, having obtained a protection with an areal density of 35 kg/m^2 able to prevent perforation to a threat of NIJ Grade IV. It is worth again noting that a saving in weight of 15–20% compared to conventional reinforcement in

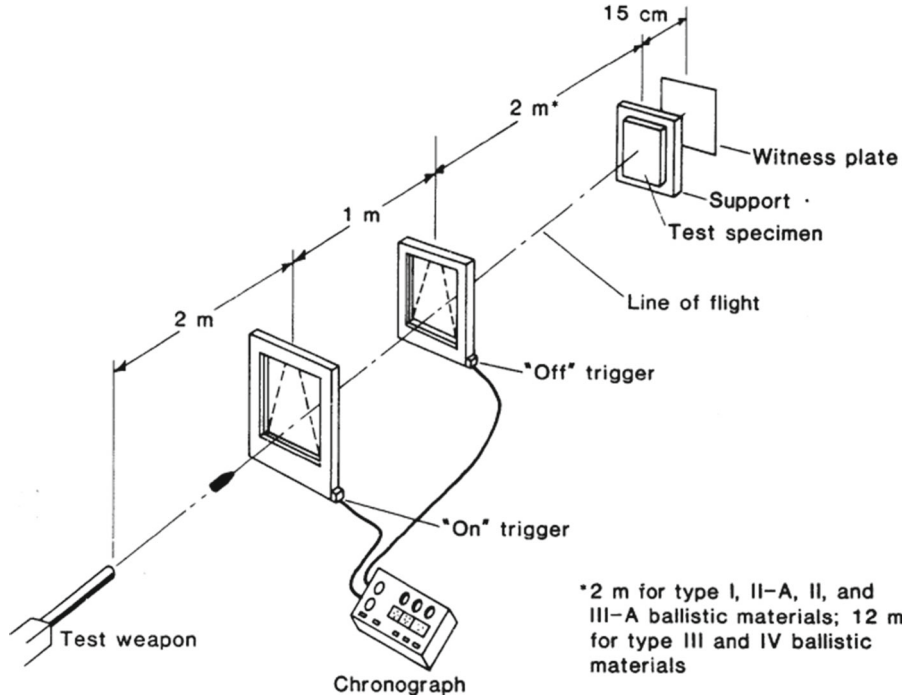

Fig. 4 Setting ballistic tests (Reproduced with permission from [22])

Fig. 5 Rigid structure for fixing the target panel edges

composite armors as reported in the literature has been obtained (see, e.g., [14]).

One panel was tested with the presence of a clay layer in the back of the target in order to evaluate the dynamic damage effect of the impact. This makes possible to assess the actual deflection extension of the dynamic impact suffered by a rear structure.

The test effect on the clay, shown in Fig. 7, is represented by the penetration of the panel inside the clay layer in the shape of three spherical recesses. It was then measured the maximum penetration for each impact inside the clay by a digital caliper, and the penetrations were measured in the range of 30 mm.

3.2 Specimens examinations

Once completed experimental tests, the panels became the subject of nondestructive and destructive analyses aimed at obtaining the characterization of the different types of damages and fractures due to the impact into ceramic materials and into back-packing. These analyses also allowed displaying and defining the actual mechanism of penetration of the projectile inside the composite material.

At first, each specimen was firstly subjected to radiographic analysis aimed at obtaining the size of the holes of the projectile, the breakage of the small panels of ceramic material, the propagations of the fractures within the ceramic material and the fragmentation of the projectile. In addition, for each tested panel,

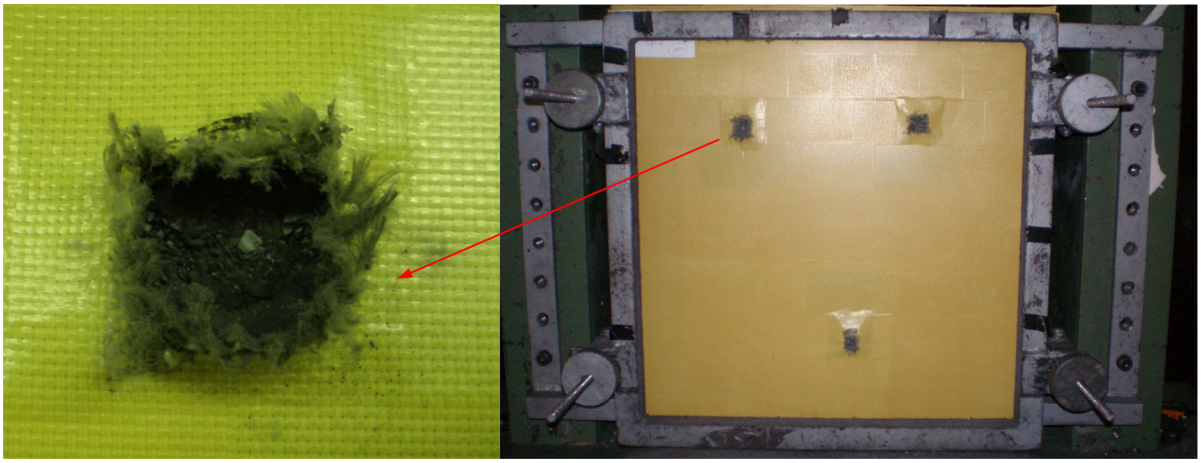

Fig. 6 Strikes on tested panel

a three-dimensional scan of the external geometry was performed, from which the detailed extent of the damage and the total deflection of the bulge of the panel back side are obtained, assessing quite accurately the effect of the impact of the bullets.

Once concluded the nondestructive analysis on individual panels, at the Marine Structures Testing Lab of DITEN, all destructive analysis were conducted with the purpose of obtaining further information about the kinds of fractures and on their propagation within the various materials and also to visually confirm the nondestructive evaluations about the penetration of the projectile inside the panel.

Table 2 Experimental results and damage caused by the shot (CP = complete penetration, H = hold)

Panels	Panel no.	Impact	Results
SiC-HB26	Panel 1	Test 1	CP
		Test 2	H
		Test 3	H
	Panel 2	Test 1	H
		Test 2	H
		Test 3	H
	Panel 3	Test 1	H
		Test 2	H
		Test 3	H

3.2.1 Radiographic analysis

The X-ray analyses allow evaluating the structural integrity of each tile of ceramic material and in particular to verify the breakage and fracture propagation after the bullet impact, during the ballistic tests. However, a limitation of the radiographic analysis was due to the presence of the ceramic layer itself on the panels: As a matter of fact, the evaluation of the delamination phenomena on the rear Dyneema® back-packing was not possible. Nevertheless, this analysis allowed verifying, with significant accuracy, the penetration hole size of the projectiles, the breakage of the ceramic tiles and the propagation of the fractures inside the adjacent tiles. In all radiographs, whose Fig. 8 is an example, the following types of damages can be displayed and highlighted:

- Fragmentation of the central core of the projectile and dispersion of the fragments, a phenomenon greatly highlighted by the presence of a clearer "cloud" in the images, which defines in fact the propagation of fragments and steel powders of high density as far as an increased absorption of the X-ray is caused by the higher density of the material;
- Complete rupture of the ceramic tiles on which the impact takes place, evidenced by the more definite color of the tile and by the presence of small size fragments;
- Damage propagation on adjacent tiles (including white alumina tiles);

X-ray images obtained were later compared with the pictures obtained from the destructive tests of the pan-

Fig. 7 Impact test with modeling clay on its rear

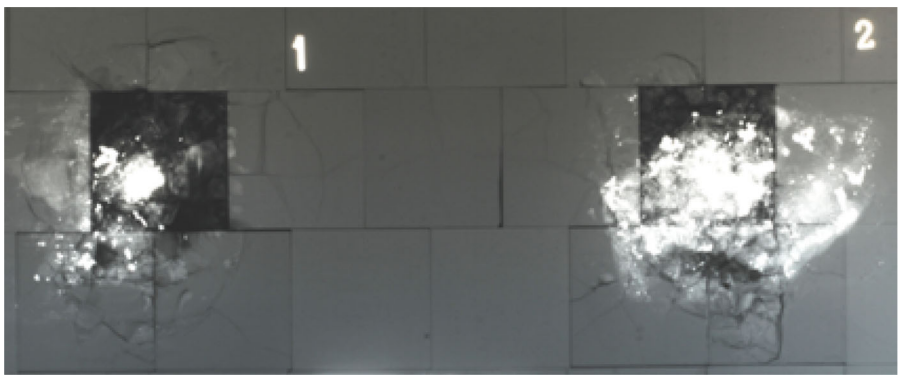

Fig. 8 Panel radiography, complete brake, and fragmentation of the SiC tile impacted

els: The comparison is useful to support and complete the analyses of some cases difficult to be interpreted.

3.2.2 Tri-dimensional scan

The extension of the panel maximum back-packing deflection in way of the bullet point of impact and the extension of the damage areas on front and rear surfaces for each point of impact appear to be of paramount importance for the comparison between the ballistic tests results and the numerical simulations. The panels were then scanned to provide information necessary for the comparison. Accurate geometry of each tested specimen was obtained by means of a three-dimensional scanner without any contact possibly affecting the surface shape; see Fig. 9. A CAD model was obtained where the scan information is summarized and stored.

Taking advantage of the accurate CAD model of the scanned surfaces, quantitative information was obtained such as the maximum extension of the residual rear deflection in way of the bulge, the deformation of the front surface of the panel, and the different shapes and sizes of the damaged areas (Fig. 10).

3.2.3 Destructive analyses

All the observations made during the phases of destructive analysis conducted at the DITEN Marine Structures Testing Lab are described in the following. They allowed evaluating and defining the size of the different types of damages and fractures occurred in the material.

The tested panels have been subject to a detailed photographic analysis of the damage extension due to the bullet impact on the back surface and the front plate before any destructive analysis (Fig. 11).

The main damage dimensions measured during the nondestructive analyses were also confirmed for each point of impact from photos and direct measurements as

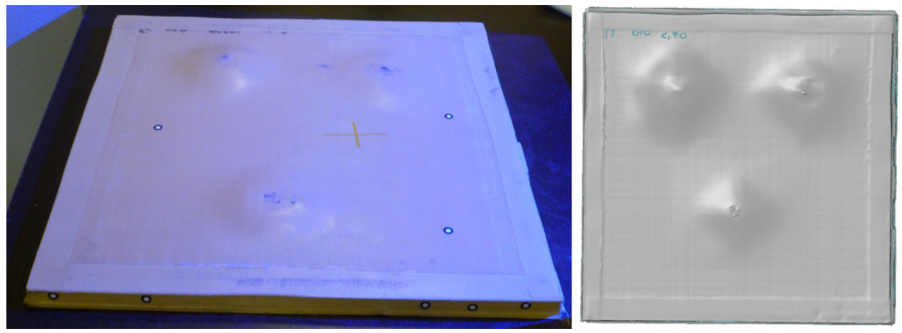

Fig. 9 Acquisition of three-dimensional scans

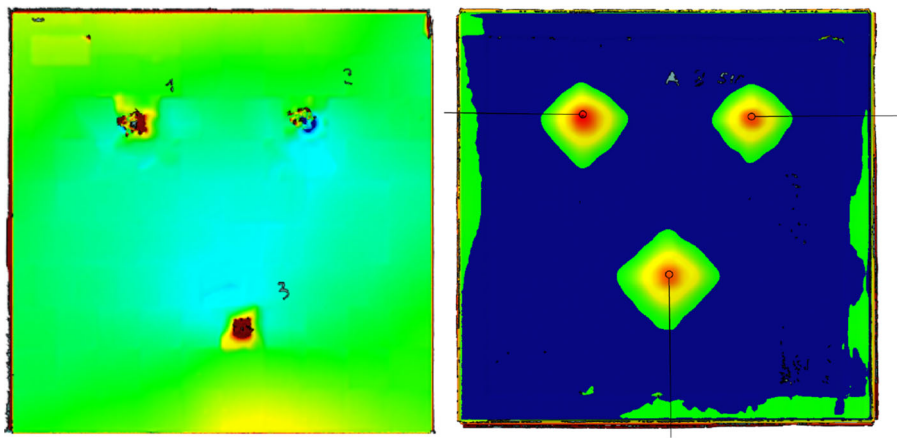

Fig. 10 Tri-dimensional scan of the impact target (front and rear)

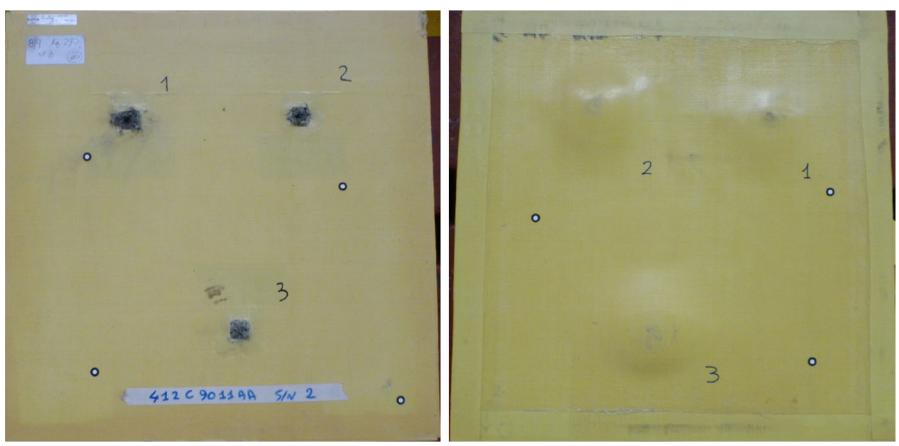

Fig. 11 Front and rear of a tested panel before destructive tests

reported in Table 3. The results reported are normalized with respect to the real dimension of the square ceramic tiles due to confidentiality.

After completely removing the protective top layer, the breaks and fractures involving the ceramic layers are revealed: Figure 12 shows images of the interior of a panel with cracks in the SiC tiles: Damage caused by the impact is clearly visible, and even the location and extension of the damage over the entire panel surface are visible.

Figure 13 compares the radiographic images with the ones obtained from destructive tests after removal of the protective top layer. After carefully removing the ceramic debris, the true size of the damage extension on the impacted tiles appear. The extent of fractures on the impacted tile and on the adjacent ones allow evaluating the damage propagation and the different type of

Table 3 Main dimension of impact holes in the tested panels (normalized)

Type	Panel	Shoot no.	Ø holes	Est. front damage		Est. rear damage		Results
				HOR.	VERT.	HOR.	VERT.	
–	–	No.	%	%	%	%	%	
Main dimension holes								
SiC - HB26	412C 9011AA SIN 1	1	44.0	106.0	110.0	154.0	142.0	Hold
		2	38.0	108.0	104.0	174.0	160.0	Hold
		3	46.0	162.0	110.0	154.0	148.0	Hold
	412C 9011AA SIN 2	1	56.0	108.0	100.0	248.0	238.0	Hold
		2	50.0	80.0	96.0	268.0	288.0	Hold
		3	44.0	100.0	110.0	274.0	256.0	Hold
	412C 9011AA SIN 3	1	58.0	142.0	132.0	254.0	262.0	Perforation
		2	24.0	114.0	144.0	240.0	226.0	Hold
		3	56.0	106.0	112.0	216.0	196.0	Hold

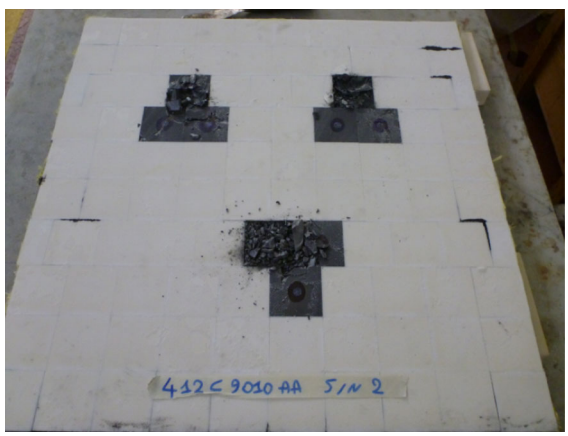

Fig. 12 Ceramic tiles on the panel after top protection removal

penetration of the projectile: The main dimensions of the damage and fracture due to the impact were measured as per Table 4, and the internal penetration of the bullet are referred to the armor total thickness.

The removal of ceramic tiles from the panel allows evaluating and analyzing the deformation of rear back-packing. It was possible to determine the geometrical dimensions of the extensions of the front damage and the projectile perforation inside the material, Fig. 14.

For all the impact points, detailed investigations related to the geometry of the entry wound of the bullet, the extension of the deflection on the back-packing back, and damage the fibers in the area of impact were carried out. In Fig. 15, two images of the damage caused by the impact of the bullet are shown: The geometry of the hole is rectangular, and the fibers inside the impact hole are burned during the penetration.

Table 5 shows the main dimensions of the holes referred to the real dimension of the ceramic tiles: In particular, the vertical and horizontal extension of the penetration damage on the ceramic tiles and the extension of the damage on the front surface of the panel were carefully measured. In addition to the hole diameter, also the internal penetration and the real bulging are reported normalized with respect to the total amour thickness.

During the destructive analyses of the impacts on rear back-packing, it was possible to extract, at impacts not fully penetrated, the central cores of the 7.62 M2 bullets and portions of their outer covering brass: It is useful the evaluation of the type of fracture and breakage of the projectile during the ballistic impact. All the bullets were analyzed, and results are the starting basis for subsequent numerical simulations. Figure 16 shows an example of extracted bullet portions.

From the analysis, actual characteristics of the deformation of the bullet due to the impact are drawn out as follows:

- Breaking and brittle deformation of the high-strength steel core: All the specimens show breakage typical of fragile material as expected due to erosion of the bullet.
- Presence of metal debris from eroded projectile inside the points of impact: All these compounds have a small size of 1–2 mm at most.

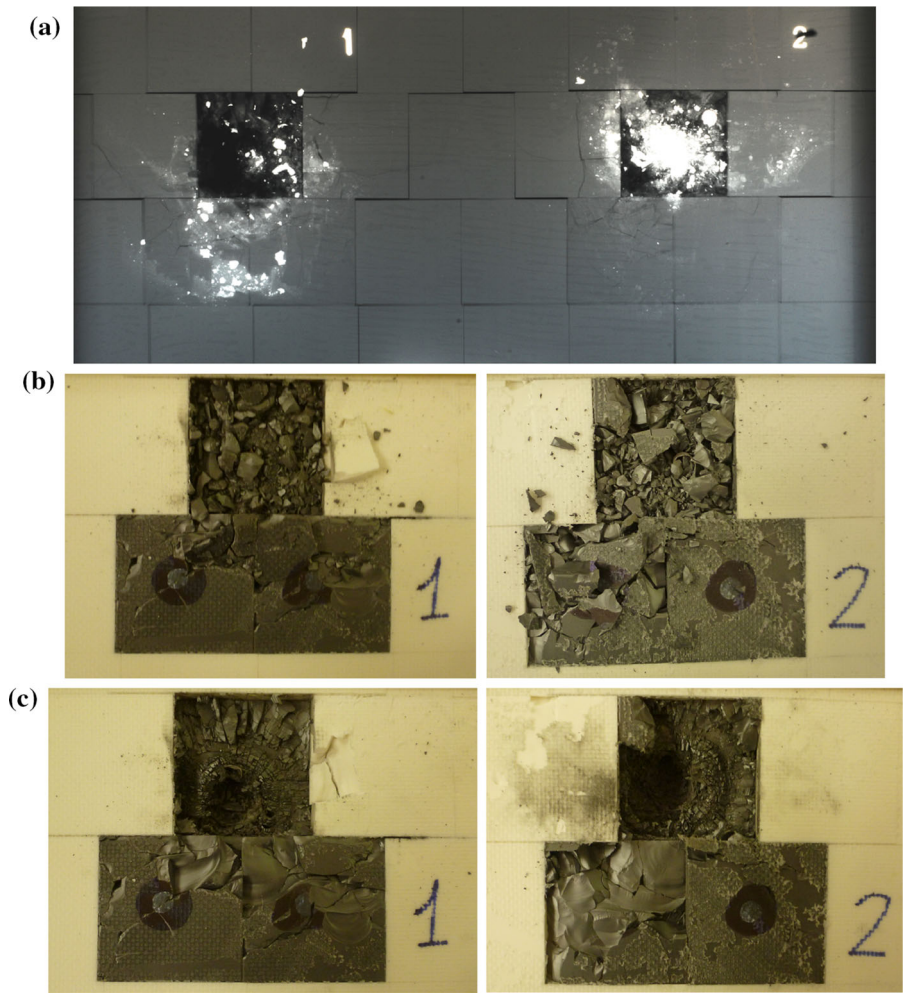

Fig. 13 Radiographic analysis **a** compared with real tears with (**b**) and without (**c**) ceramic debris. *Note* X-ray image from opposite side

Table 4 Ceramic layer damage dimension

Type	Panels	No. hole	Ø hole	Est. tiles damage		Est. fracture propagation		Internal penetration
				HOR.	VERT.	HOR.	VERT.	
–	–	No.	%	%	%	%	%	%
SiC-HB26	412C 9011AA SIN 1	1	24.0	142.0	172.0	SiC only	SiC only	100.0
		2	14.0	154.0	176.0	202.00	SiC only	120.0
		3	20.0	150.0	100.0	180.00	SiC only	105.0
	412C 9011AA SIN 2	1	24.0	202.0	186.0	SiC only	SiC only	105.0
		2	52.0	150.0	202.0	SiC only	SiC only	130.0
		3	42.0	100.0	100.0	SiC only	SiC only	110.0
	412C 9011AA SIN 3	1	//	1	1	220.0	200.0	//
		2	//	1	1	120.0	200.0	//
		3	//	1	1	220.0	140.0	//

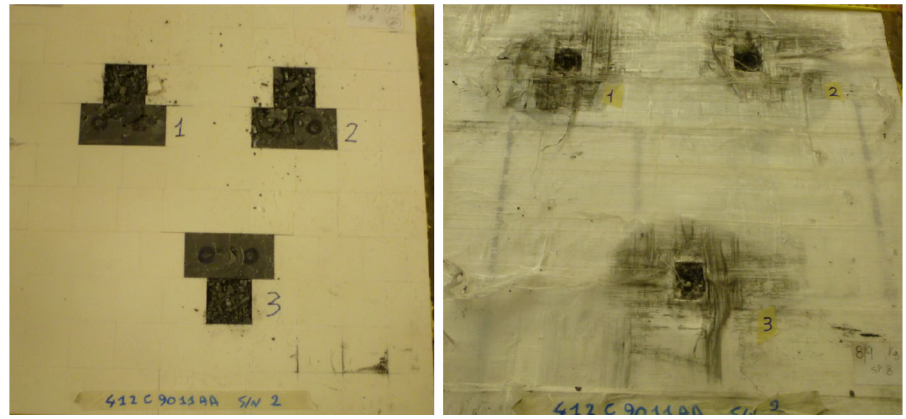

Fig. 14 Front face and rear back-packing surface of a panel

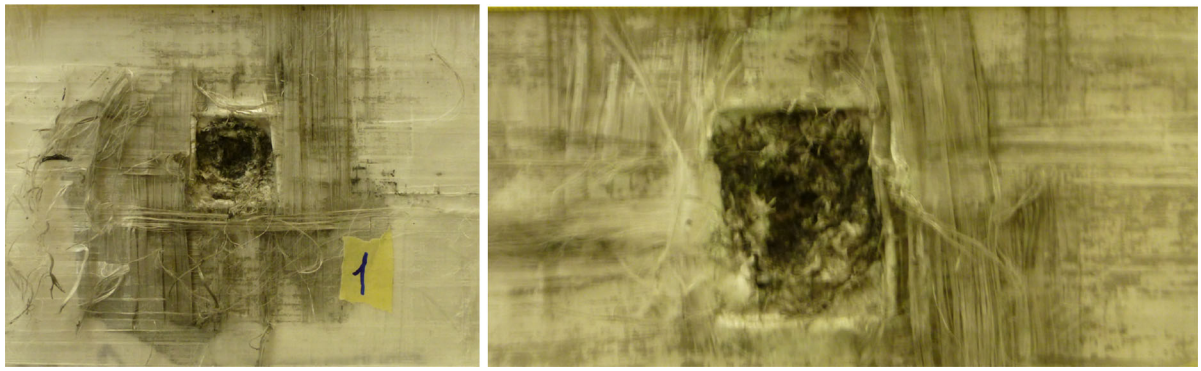

Fig. 15 Impact perforation on back-packing (front and rear sides)

Table 5 Dimension back-packing Dyneema® breaking

Type	Panel	No. hole	Ø hole	Est. damage penetration		Est. bulge propagation		Internal penetration	Rear bulging
				HOR.	VERT.	HOR.	VERT.		
		No.	%	%	%	%	%	%	%
Dimensions back-packing Dyneema breaking									
SiC-HB26	412C 9011AA SIN 1	1	26.0	52.0	60.0	150.0	126.0	100.0	260.0
		2	20.0	52.0	58.0	142.0	130.0	120.0	305.0
		3	18.0	52.0	50.0	144.0	140.0	105.0	250.0
	412C 9011AA SIN 2	1	30.0	62.0	68.0	238.0	230.0	105.0	410.0
		2	26.0	64.0	76.0	214.0	224.0	130.0	620.0
		3	24.0	62.0	74.0	270.0	204.0	110.0	450.0
	412C 9011AA SIN 3	1	18.0	66.0	64.0	202.0	196.0	//	560.0
		2	12.0	74.0	70.0	216.0	220.0	//	470.0
		3	14.0	70.0	60.0	52.0	140.0	//	430.0

Fig. 16 Extractions of bullets and their outer coating

- The outer brass is deformed, completely folded back on itself, and remains stuck in the panel during the penetration of the projectile.
- Note the separation of "caps" back of the brass coating that looks undeformed after the impact.

3.3 Ballistic tests summary

During the tests, breaking behavior of the ceramic material was obtained despite its interpretation is rather complex. Moreover, the Dyneema® back-packing behavior has been characterized, which was not reported in previous works in open literature to the best of the authors' knowledge; only in O'Masta et al. [24] and Fallah et al. [5] the rupture of Dyneema® fibers due to blast or different impact events is indeed addressed. All this information was used to validate the simulation by matching the deformation of the panels and the extension of the damage (Table 6).

3.3.1 Geometry and size of the damage

The damage generated by the impact of the projectile on the front surface of the panel appears to be limited, well defined, and visible; the entry wound of the bullet has a diameter ranging from 1.2 to 2.9 mm. In Table 5, the damage parameters are shown.

The maximum static deflection detected by the non-destructive analysis highlighted a static bulging up to six times lower than the maximum dynamic deflection imprinted on the layer of clay and due to the dynamic effects of the impact. The average penetration inside the modeling clay of the three perforations was about 30 mm, while the panels show a maximum deflection after the test of about 5–6 mm. The effect of the presence of the clay was approximately considered by engineering judgment. This information is very important to estimate the permanent damage generated on the armor protection in comparison to the total elastic one. Moreover, the protected structure laminated or fixed directly onto the ballistic protection is affected by the total deflection of the armor, even if the armor deformation itself is lowered after the impact

3.3.2 Dyneema® back-packing analysis

The damage and penetration of the projectile into the back-packing were analyzed in all the impact points (see Fig. 17):

- The breakage of the fibers at the point of impact is defined by a square geometry having a constant size of the order of 3 cm for all the impact points.
- The entrance hole of the bullet presents a cylindrical geometry and a constant diameter inside the target. In the case of complete penetration, the bullet penetrates generating a cylindrical rupture of constant diameter, while for the panels which have retained the bullets penetrations assume a different configuration with a geometry that is not constant and with apparent signs of burning in the internal fibers.
- Inside the point of impact, the fibers appear to be completely burned and damaged as a result of the penetration of the projectile inside the panel.
- The damage area on the front of the panel extends on average for a circular area having a diameter of 9–10 cm.
- The penetration of the projectile inside the panel causes a localized damage, small in size compared to the damage caused on the upper ceramic layer; also the damage is caused only within the fibers and not on the surface layer.

Table 6 Dyneema® Hard Ballistic 26 mechanical properties (Reproduced with permission from [20])

Orthotropic linear elastic model			Effective stress–strain $\sigma-\varepsilon$ values			Plasticity coefficients			Effective stress–strain $\sigma-\varepsilon$ values		
E_{11}	3.62	[Gpa]	$\sigma_{eff\#1}$	1.76E+02	[kPa]			Unit t			Unit
E_{22}	26.9	[Gpa]	$\sigma_{eff\#2}$	9.89E+02	[kPa]	a_{11}	3.00E−02	[–]	σ_{11fail}	1.07	[Mpa]
E_{33}	26.9	[Gpa]	$\sigma_{eff\#3}$	1.74E+03	[kPa]	a_{22}	1.00E−05	[–]	σ_{22fail}	753	[Mpa]
ν_{12}	0.013	[–]	$\sigma_{eff\#4}$	2.42E+03	[kPa]	a_{33}	1.00E−05	[–]	σ_{33fail}	753	[Mpa]
ν_{23}	0	[–]	$\sigma_{eff\#5}$	3.10E+03	[kPa]	a_{12}	1.00E−06	[–]	τ_{12fail}	1.01E+20	[Mpa]
ν_{31}	0.5	[–]	$\sigma_{eff\#6}$	5.97E+03	[kPa]	a_{13}	1.00E−06	[–]	τ_{23fail}	35.2	[Mpa]
G_{12}	30.7	[Mpa]	$\sigma_{eff\#7}$	1.20E+04	[kPa]	a_{23}	1.00E−06	[–]	τ_{31fail}	1.01E+20	[Mpa]
G_{23}	42.3	[Mpa]	$\sigma_{eff\#8}$	2.07E+04	[kPa]	a_{44}	1.00	[–]	$_{c11}$	790	(J/m^2)
G_{31}	30.7	[Mpa]	$\sigma_{eff\#9}$	3.46E+04	[kPa]	a_{55}	1.75	[–]	G_{c33}	30	(J/m^2)
Polynomial EOS			$\sigma_{eff\#10}$	2.02E+08	[kPa]	a_{66}	1.75	[–]	G_{c22}	30	(J/m^2)
A_1	7.04	[Gpa]	$\varepsilon_{eff\#1}$	1.82E−04	[–]				G_{c31}	1.46	(J/m^2)
A_2	10	[Gpa]	$\varepsilon_{eff\#2}$	1.20E−03	[–]				G_{c12}	1.46	(J/m^2)
A_3	0	[Gpa]	$\varepsilon_{eff\#3}$	3.11E−03	[–]				G_{c23}	1.46	(J/m^2)
B_0	3.864	[–]	$\varepsilon_{eff\#4}$	6.92E−03	[–]				Damage coupling	0.5	(kPa)
B_1	3.864	[–]	$\varepsilon_{eff\#5}$	1.13E−02	[–]						
T_1	7.04	[Gpa]	$\varepsilon_{eff\#6}$	2.83E−02	[–]						
T_2	0	[Gpa]	$\varepsilon_{eff\#7}$	5.78E−02	[–]						
T_{ref}	293	[K]	$\varepsilon_{eff\#8}$	1.06E−01	[–]						
Specific heat	1850	[J/kgK]	$\varepsilon_{eff\#9}$	1.061E−01	[–]						
Thermal cond.	0	[J/mKs]	$\varepsilon_{eff\#10}$	1	[–]						

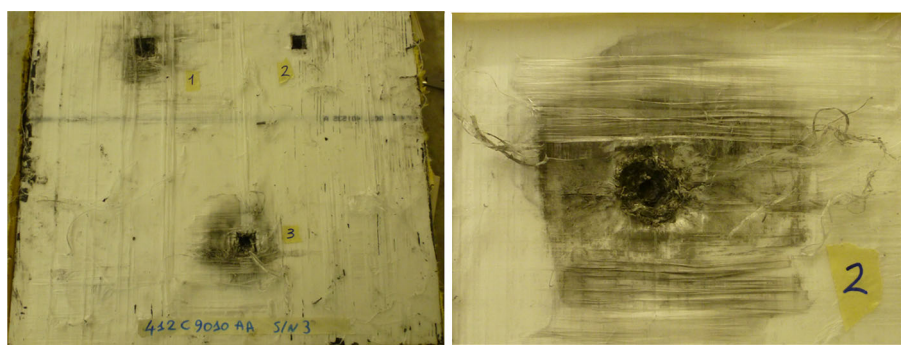

Fig. 17 Penetration of the bullet from the rear back-packing

4 Numerical simulation

4.1 Introduction

The numerical methods used for the solution of the ballistic problems involve finite difference, finite volume, and finite element approaches as well as meshless approaches. The choice of the applied method depends on the physical nature of the problem being studied; see [12].

For numerical simulations of the ballistic problem, the software available to the company OTO Melara is the explicit dynamic solver Ansys-AUTODYN®, which allows modeling the nonlinear dynamics of solids, fluids, gases, and their interactions suitably selecting one or more of the above-mentioned approaches. This software was found very appropriate for the simulation of high-speed impacts, both for anti-ballistic impacts and for hyper-speed impacts typical of space debris.

The solution of the explicit dynamics allows simulating the mechanical behavior of nonlinear structures during physical events occurring in very short time, approximately a few milliseconds or even less. All these events are dominated by transient behavior of stresses and strains. The main characteristics of the materials are defined by constitutive equations and kinematic equations that describe the dynamic behavior and interactions between strains, stresses and the whole energy of the involved materials. The explicit dynamic simulation is partially implemented and developed as hydrocodes or SPH (Smoothed Particles Hydrodynamic) codes. In particular, the projectile is defined by SPH particles, while the armor system is FEM simulated. The so-called hydrocodes offer an interesting alternative approach to large deformation problems since the lack of a grid removes the need for unphysical erosion algorithm; they are typical dynamic software, particularly suited for modeling impact, penetration, and blast events [3].

Additional methods are available in the solver AUTODYN®, e.g., it is possible to select among different types of traditional finite element discretization of the problem according to the Lagrangian scheme, the Eulerian scheme, and the arbitrary Lagrangian–Eulerian (ALE) approach, in addition to the discretization of continuum particles through the SPH method.

The discretization of solid continuum and structures in the explicit dynamic physic usually takes place through a Lagrangian calculation scheme, in which each body is discretized in a mesh of fixed elements (body fitted mesh), integral with the modeled solid. The Lagrangian solution approach is the most efficient and accurate solution for almost all structural models. However, being the mesh fitted in the modeled solid, large deformation may lead to distorted elements and numerical instabilities. The SPH method is a relatively new mesh-free modeling technique, developed to solve the limitation of the finite element method due to excessive distortion of the mesh. The major advantage of this technique appears to be the lack of numerical grid required for the calculation of the spatial derivatives. It does not entail the use of an unphysical erosion algorithm for the removal of highly distorted grids to help the numerical procedure convergence [12].

4.2 Numerical model

Following the results obtained from previous simulations and experience gained during the research activity reported in Sabadin et al. [28], it was decided to apply a new modeling strategy. The model was developed through a three-dimensional modeling (3D) that allows assessing more accurately the deformation and breakage of the bullet materials and, at the same time, the propagation of cracks and fractures in the ceramic material and the deformation of the rear fibers of Dyneema®. The availability of adequate computing power and the ability to parallelize the simulation on all processors in the available workstations allowed obtaining the computations in reasonable time.

The geometry of the bullet and the target permit to reduce the total element number due to their axisymmetric geometry, modeling only a quarter of the projectile and of the target and properly setting the symmetry conditions on the edge surfaces of the target.

It was also chosen to model the entire bullets using SPH elements: This choice was dictated by the need to obtain an accurate simulation of the failure behavior of the projectile during the panel penetration. By using Lagrangian elements, in fact, plastic deformations of the core part of the bullet was reported that does not properly match the experimental results. By using the SPH elements, it is possible to estimate both the deformation of the projectile inside the panel and the dispersion of the metal fragments produced during the erosion of the ceramic layer. Moreover, symmetry conditions can be correctly defined in SPH simulations by suitably defining the simulation domain boundaries and appropriate conditions for particles in way.

As regards the target, instead, it was preferred to use more traditional Lagrangian finite elements. Both, the static and dynamic mechanical properties of the materials are well defined as far as previous simulations already provided excellent results for this modeling strategy. It was already proved in Sabadin et al. [28] that by using common Lagrangian elements it is possible to easily evaluate the propagation of fractures in the ceramic layer as the penetration of the projectile takes place thanks to appropriate erosion algorithms. However, the modeling of the rear back-packing material with Lagrangian elements was rather challenging since the dynamic mechanical properties of Dyneema® are not easy to assess. Recently, Lässig et al. [20] suitably described the behavior of Dyneema® laminates by

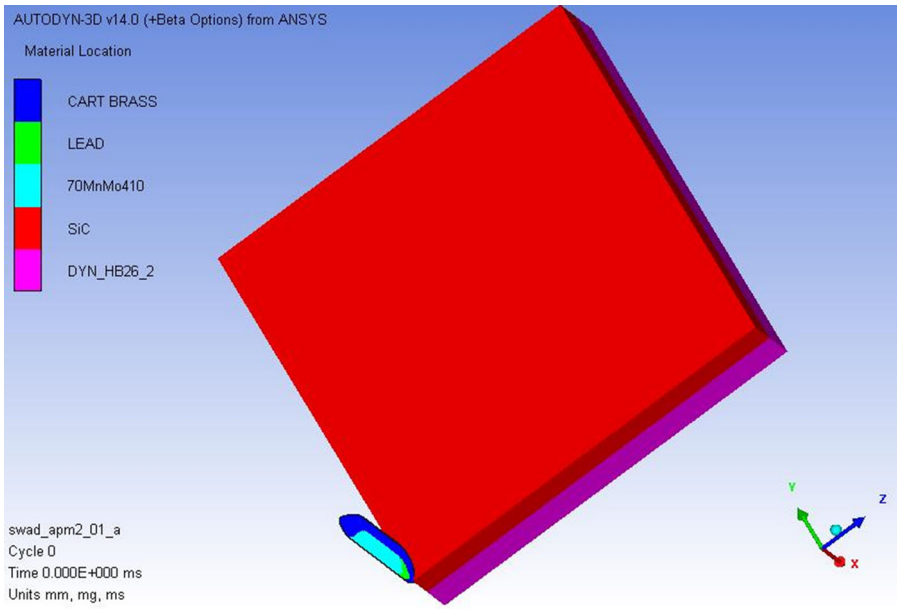

Fig. 18 Geometry of the whole numerical model

means of Lagrangian elements, and therefore reference was made to this pioneering work. In this case, symmetry conditions should be carefully defined in all layers of the finite element model also considering transient deformation behavior on symmetry planes (Fig. 18).

The numerical model simulation is eventually defined by 311,536 elements, among which 40,064 are SPH particles elements and a total of 271,472 are Lagrangian elements.

The main dimensions of the bullet and target geometry implemented in the model are reported in Fig. 19, where the discretization of their volume is also shown. To proper modeling the bullet geometry and the position of the different materials, particular attention was paid in the model definition.

4.2.1 Bullet geometry

As mentioned, the modeled threat is the cartridge caliber 30-06 SPRG M2. In the simulation, only the geometry of the bullet is defined: The bullet is made of three different materials, a central core made of high hardness steel with a lead tip, all covered by a copper alloy outer jacket. The mechanical materials properties are chosen from the AUTODYN® internal library.

The bullet has a total length of 35.1 mm and a maximum outer diameter of 7.77 mm. The core geometry is an important part of the bullet, governing the penetration mechanism inside the target panel. A total of 40,064 SPH particle elements were used in total for the definition of the projectile, having each an outer diameter of 0.1 mm (initial distance from other particles). The bullet mesh size was selected after a careful sensitivity analysis, and it is deemed optimal to highlight the materials failure behavior and the deformation of all the individual components of the projectile. 17,369 elements form the outer jacket brass (dark blue), 20,629 elements the high hardness steel core (blue) and, finally, the lead cap is defined by 2066 elements. Mechanical properties of each material are described by equations describing the interaction among particles and with domain boundaries.

4.2.2 Target geometry

Two different rigidly connected composite materials make up the target panel: For this reason, two different groups of three-dimensional Lagrangian finite elements were defined, one for the ceramic layer and one for the rear back-packing, whose geometry was modeled considering the layers' properties and thickness using layered shell finite elements as available in the software (Fig. 20).

The target model is constituted by three-dimensional elements fitted into a 100 mm square of variable thickness subdivided as shown in Fig. 21. The element size was evaluated based on experimental results and represents the minimum target amplitude that allows assess-

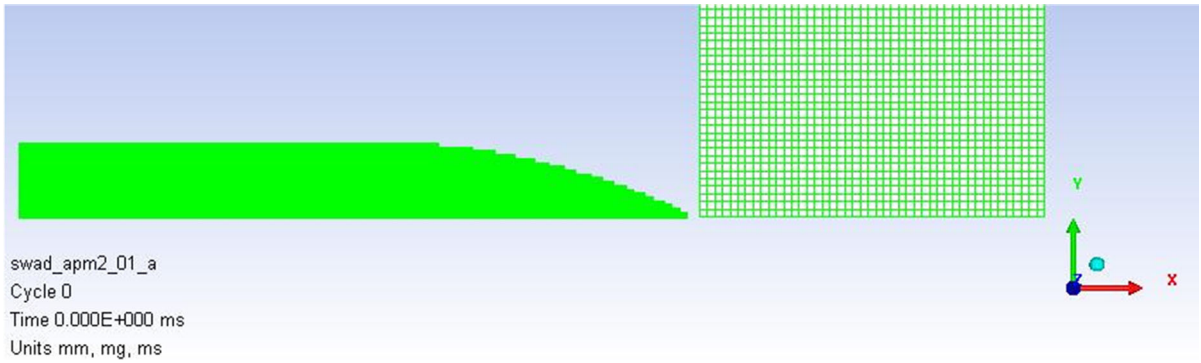

Fig. 19 Model geometry and mesh subdivision

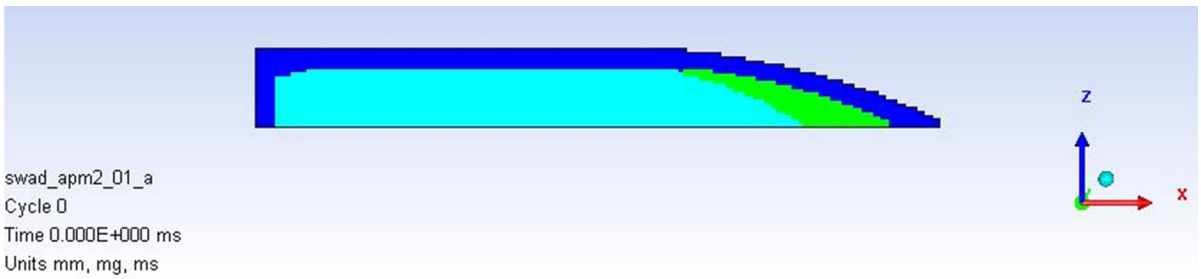

Fig. 20 Bullet mesh subdivision

ing the whole extension of the rear bulge resulting after the penetration of the projectile. Furthermore, with this element size, the breakage of ceramic tile surrounding the point of impact can be estimated.

To decrease the total elements number in the model, only 75 elements on each side of the target were used, with variable length size. The element density of the target geometry was refined in the surrounding area of the bullet impact point, thus creating a non-uniform mesh, as shown in Fig. 21.

Symmetry boundary conditions were applied on layered shell elements

4.3 Simulation parameters setting

The key parameters for proper simulation configuration of the bullet impact on the target are described in the following. It is assumed that the projectile hits the target at a specific initial velocity, while the target composite layer edges are fully constrained.

The boundary conditions are applied to the end nodes of the rear part of the target geometry (i.e., the edge of the back surface), in particular by imposing null velocity (and displacements) values in all directions (i.e., degree of freedom, DoF) of the nodes of the Dyneema® fibers. It means that the bottom of the composite surface edges of the target geometry is completely constrained, but the edge surfaces of the ceramic layer are left free as shown in Fig. 22. The bullet initial velocity was also defined, and this speed is assumed constant on all the SPH elements of the bullet: A constant speed of about 850 m/s, along the X axis which represents the average speed of experimental ballistic impact, was imposed. Different parts of the model were joined together by appropriate constraints available in the software environment. If two parts are joined, the software automatically identifies and joins all DoF of coincident nodes of the two distinct parts [2]. The loads and relevant boundary conditions are therefore properly transferred between elements having different characteristics, in this case between the ceramic layer elements and the fibers package elements.

The duration of the numerical simulation and the time step are key parameters of the simulation. The following values were found satisfactory for the captioned case: 1,000,000 steps of 0.2 ms each. These values were found to be consistent with the duration of target penetration and with the maximum number

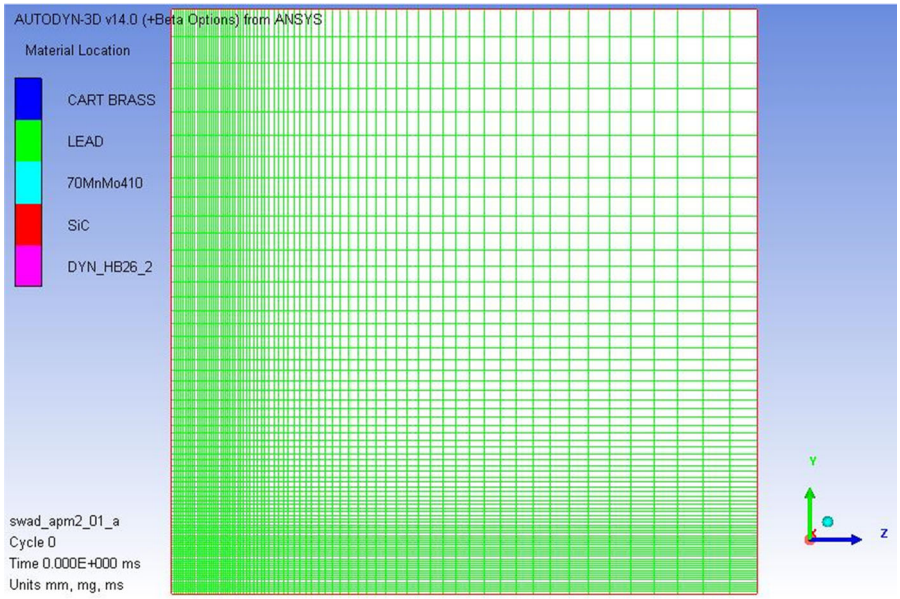

Fig. 21 Target mesh discretization

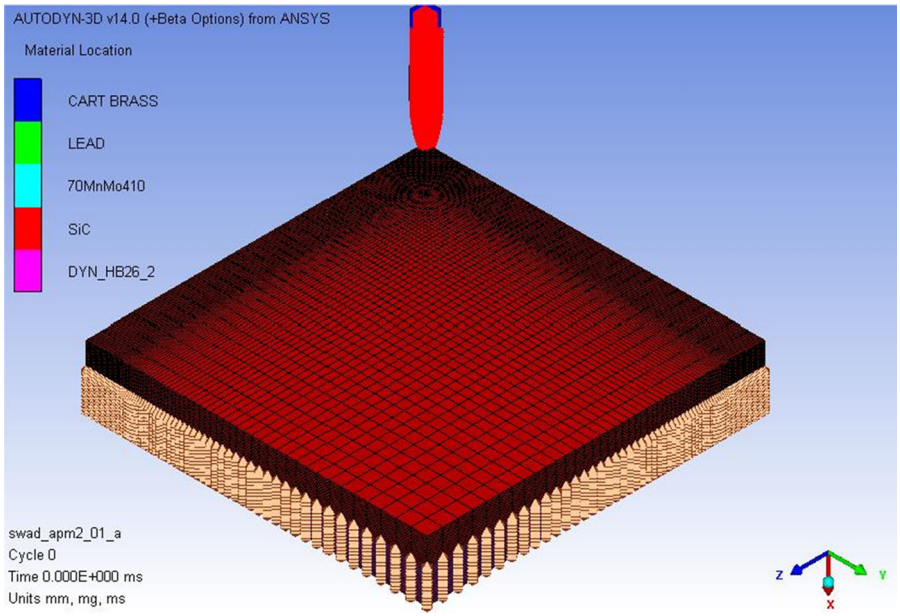

Fig. 22 Boundary conditions definition

of cycles necessary for the development of the entire three-dimensional simulation. In certain simulations, it was subsequently decided to increase the value of the time step bringing it up to a maximum of 0.25 ms in order to obtain a larger amount of information on the deceleration of the projectile inside the target simulating a longer event. To reduce the computational cost, it was decided to set a maximum element speed equal to 20,000 m/s. This setting results in the deletion of the SPH elements that, after the panel impact, become fragments and greatly increase their speed, but they are no longer useful for the purposes of the simulation, i.e., the penetration of the projectile, so reducing the computation costs.

5 Material characterization

The used dynamic solver allows implementing the behavior of materials subjected to high dynamic loads

through appropriate constitutive models. The material models definitions were implemented into separate set of equations as follows [2]:

- Equation of state: defines the relation between the hydrostatic pressure, the local density, and local specific energy of the material.
- Strength equation: describes the materials behavior, in particular the deformation during the high dynamic loads application. Basically, the stress–strain relationships are set.
- Failure mode: simulates the various ways in which materials fail under extreme loading conditions, resulting in crushed or cracked materials, considering the above-mentioned set of equations and relevant variables.
- Erosion algorithm: It is a numerical mechanism for the automatic removal (deletion) of elements during a simulation. Erosion can be used to allow the simulation of material fracture and penetration, removing very distorted elements before they degenerate. The stresses associated to deleted nodes are transferred to remaining nodes.

While dynamic characterization of other materials is available in [2], the ballistic impact simulation on composite Dyneema® has been possible thanks to an intensive literature survey aimed at finding dynamic mechanical properties of this composite material.

5.1 Metallic materials

For metallic materials considered in the numerical simulation such as steel, lead, and brass, a simple linear equation of state linking pressure and internal volume variations is used:

$$P = K\mu. \tag{1}$$

where $\mu = \frac{\rho}{\rho_0} - 1$ is the compression coefficient, being ρ_0 the initial density, ρ the current density, and K the bulk modulus. To represent the constitutive response of metallic material models subjected to deviatoric strains, it is used the model of Johnson–Cook presented in [17]. Reference was made to data of a steel alloy, made available from prior research by OTO Melara. This material is described by a "shock" equation of state (EoS); the stiffness is provided according to the Johnson–Cook equation.

The mechanical properties of the materials used for the cap, namely brass and the lead, have been selected in the software material library: Considering the experience gained in the simulation of dynamic impacts, the two materials guaranteed good numerical results. Cartbrass material was exterior brass defined through a "shock" EoS and again by Johnson–Cook constitutive model, while the lead material used for the inner part was defined by a "shock" EoS and a different constitutive model, defined by Steinberg–Guinan strength equation [29].

The a.m. metallic materials are used to characterize SPH particle elements, so they do not require an erosion algorithm to allow the correct simulation performance, removing mesh elements too distorted: This allows obtaining a more accurate simulation regarding the bullet damage inside the target and the fragments propagation generated during the ogive erosion.

5.2 Ceramic material

To describe the mechanical behavior of the ceramic materials, particularly of the SiC layer, a polynomial EoS is used in which the relationship between pressure, density, and value of internal energy is set considering the intact model. Inside the ceramic materials, when the damage begins to occur due to the action of external loads, it is possible to have bulking phenomena. The effect of bulking occurring in brittle materials is to increase the internal pressure while keeping constant the volumetric density and/or increase the volumetric strain, maintaining constant the pressure. For the full definition of Johnson–Holmquist constitutive equations and damage model, reference was made to the implementation of this relation in Holmquist and Johnson [15].

The SiC ceramic material model available in the Autodyn® materials library is used in all the simulations. The constitutive properties and the damage equations are defined by the JH-1 Johnson–Holmquist equation. The description of the ceramic materials through Johnson–Holmquist equations implementation is known to be correct and of common use in the simulation of dynamic events.

In addition to the dynamic mechanical properties of the material, the so-called instant erosion algorithm was also defined, being Lagrangian elements still applied [2]. These equations were set after careful sensitivity analyses. In particular, the geometric strain erosion model is used in this work, and the maximum geo-

metric strain of each individual element is computed according to all the strain components.

5.3 Orthotropic material

Specific attention was paid to the mechanical characterization of Dyneema® fiber-reinforced laminates, in our case of the Dyneema® Hard Ballistic 26 fibers. In the software library, the physical parameters of such innovative material are not reported: In fact, it was manufactured and in use for production of ballistic protections only recently and, understandably, confidential in commerce.

These parameters are difficult to find out, but actually several mathematical models for defining Dyneema® behavior were developed and applied in the earlier stages of the research. The model presented by Grujicic et al. [12] partially provides the necessary parameters for Dyneema® fibers description in the software and the Dyneema® BT-10 mathematical model previously applied by OTO Melara in other studies may be adapted for the purpose. However, these mathematical models do not guarantee the correct simulation of the Dyneema® Hard Ballistic 26 behavior: In fact, the results obtained in preliminary computations are not in agreement with the experimental results of the ballistic tests.

Very recently, it has been published a comprehensive paper related to the main values of the mechanical properties of the Dyneema® Hard Ballistic 26 laminate definition [20]. The paper provides results of laboratory tests carried out for the numeric parameter validation and presents numerical values of the individual parameters necessary for material implementation.

Such material behavior is much more complex than a traditional isotropic constitutive model used in antiballistic field. Additional effects to complete the material model include:

- Anisotropy properties of the stiffness matrix of the material;
- The tensile strength/stiffness decrease due to anisotropy and the post-failure behavior of the damaged material;
- The relationship between the spherical and deviatoric component of the stress tensor;
- The nonlinearity effect in the pressure and density relationship.

Fiber composite materials mechanical responses subject to large deformations and high strain rate are defined through the orthotropic material model defined by Hayhurst et al. [13]. This material is based on the original idea proposed in Anderson et al. [1], where authors developed a theoretical approach to the material anisotropy coupling it with the nonlinear material response.

Regarding the fibrous composites, the main causes of failure due to impact loads are identified as the delamination between the layers, the shear deformations causing the matrix failure, and the fibers failure themselves. These failure modes lead to a reduction in the ability to sustain a load in one or more directions, and for this reason, this phase as well as that of softening, i.e., the reduction in the ability to support tensile stress during deflection, was considered. Other failure modes are due to the matrix fusion ("burning") and fibers degradation due to an excessive thermal gradient in the material: These effects are taken into account only in hypervelocity impacts, while they are not relevant for impacts with speeds lower than 1000 m/s, as in this case.

6 Results of the numerical simulations

All the results obtained from the numerical simulations carried out of 7.62 caliber M2 bullet impacts on antiballistic composite advanced protections are reported in the following. The obtained results overview allows evaluating mathematical and physical parameters optimization carried out in the present research, aimed at obtaining a numerical model able to simulate the experimental results. The results of each simulation are shown in Table 8 and 9, and the differences are highlighted to properly understand the numerical results obtained. As a conclusion, a comparison between the numerical solution and the experimental values is presented.

6.1 Simulations analysis

From the nine numerical simulations conducted using three-dimensional Lagrangian and SPH elements, remarkably interesting results were obtained. The numerical parameters that most influence the result of the simulation are reported in Table 7 showing

Table 7 Main simulation parameters

Simulation no.	Dyneema® material (–)	Dyneema® erosion (%)	Dyneema® thickness (%)	Ceramic erosion (%)	Ceramic thickness (%)	Target items (–)
Main parameters						
0	1	1.5	–	1.5	–	2
1	2	1.5	–	1.5	–	2
2	2	1.5	–	1.5	–	4
3	1	1.5	–	1.5	– 12.5%	2
4	1	1.5	– 30.0%	1.5	12.5%	2
5	1	1.5	–	1.5	–	1
6	2	1.5	–	1.5	–	1
7	2	2	–	2	–	2
8	2	2	10.0%	2	–	2
9	2	1.5	10.0%	2.5	–	2

Table 8 Main simulation results (bulging measured in one panel only)

Simulation no.	Simulation time (ms)	Bullet penetration (–)	Residual velocity (m/s)	Maximum bulging (%)	Damage extension (%)
Simulation results					
0	0.25	Yes	116	290.0%	240.0%
1	0.2	Yes	132	285.0%	200.0%
2	0.09	Yes	/		/
3	0.16	Yes	365		/
4	0.17	No	-	90.0%	200.0%
5	0.2	Yes	270		/
6	0.2	Yes	217		/
7	0.22	Yes	70	260.0%	240.0%
8	0.22	NO	–	235.0%	230.0%
9	0.22	Yes	70		/

Table 9 Damage size on impacted panels

Panel and simulations	No. hole	Bulging	Est. damage penetration		Est. bulge propagation		Internal penetration
	No.	(%)	HOR. (%)	VERT. (%)	HOR. (%)	VERT. (%)	(%)
Numerical and experimental results comparison							
SiC & Dyneema®	1	41.0	62.0	68.0	248.0	238.0	105.0
	2	62.0	64.0	76.0	268.0	288.0	130.0
	3	45.0	62.0	74.0	274.0	256.0	110.0
Simulation 8	1	235.0	66.0	66.0	260.0	260.0	155.0

the used values in each simulation normalized with respect to reference values. For each simulation, reference values of the materials mechanical characteristics used for the Dyneema® definition are shown: The index 1 refers to the parameters reported in Lässig et al. [19], while index 2 means the mate-

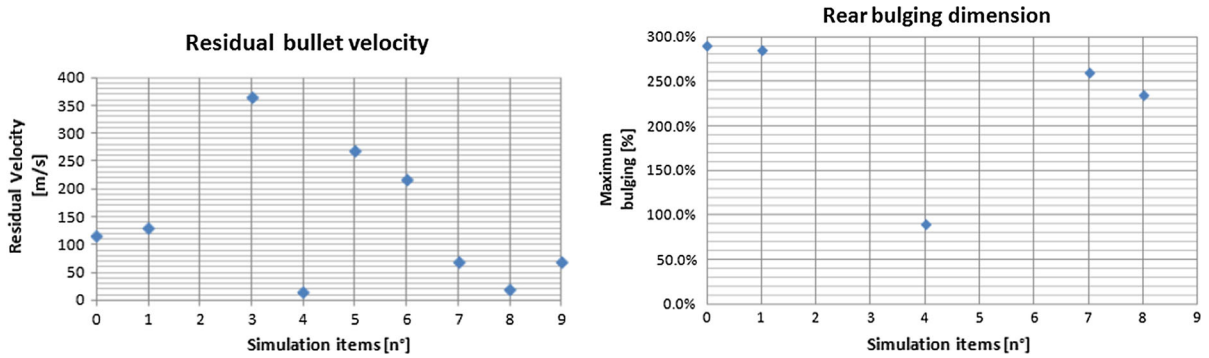

Fig. 23 Residual velocity and maximum rear bulging

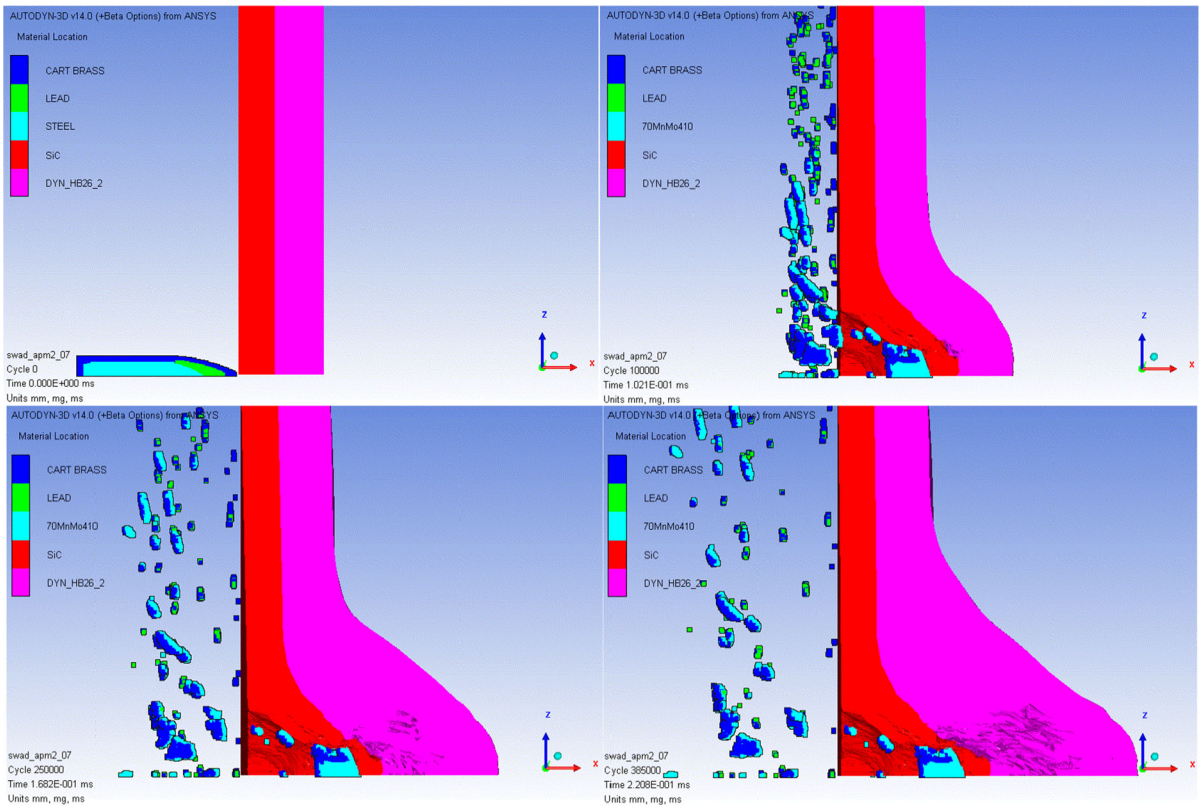

Fig. 24 Bullet penetration sequence

rials mechanical description given by Lässig et al. [20].

Simulation no. 8 represents the best numerical solution in which the most suitable numerical results in term of bullet arrest and rear panel deformation were achieved: the combination of correct thicknesses of the materials used, model geometry definition, and Dyneema® mechanical characterization allowed us to obtain excellent results.

In simulation no. 4, the material layer thicknesses were changed to verify the possibility of future development of the ballistic protection: Indeed, the simulation increasing the ceramic layer thickness and decreasing the Dyneema® one showed a remarkable improvement in term of maximum rear bulging extension due to the thickness change (Table 8).

From the results reported in Table 9, it is clear that only the simulations no. 4 and 8 reach the almost

complete bullet stop inside the amour protection: It is impossible to confirm that the complete bullet stop is reached in the simulation due to numerical difficulties preventing the conclusion of the numerical calculation, thus not allowing to obtain the desired result. In Fig. 23, the residual velocity and bulging maximum values for each simulation are shown: The smaller values of residual velocity are found for simulations no. 4 and 8, being less than 2% of the initial bullet velocity. Simulation no. 4 gets a significantly reduction of the rear bulging, that is expressed in percentage of the armor total thickness; instead, the damage extension is referred to the ceramic tile dimension.

The process conducted during this research phase has therefore resulted in an overall improvement of the geometry and of the results derived from numerical simulations: A good approximation of the ballistic tests results with regard to the bulging deformation and the extension of the ceramic cracking was obtained. Images of Fig. 24 show the rear panel deformation and the entrance hole of the bullet on the ceramic layer.

6.2 Numerical simulation validation

The numerical model used in the simulation provides elements bonding between two distinct stacked layers, ceramic, and rear fibers. Compared to previous simulations, the erosion value is changed in both materials: The geometric strain erosion is set equal to 2.0, i.e., allowing each element a maximum volumetric deformation equal to 200% of the initial dimension (before removing the element from the numerical simulation). The elements are more deformed thus absorbing more initial energy during bullet penetration. In Fig. 24, the penetration sequence in to the armor protection is reported.

Data of greatest interest in the model are the bullet velocity decrease inside the target: As shown in Fig. 25, the gauge point speed in the rear area of the projectile decreases significantly, reaching at time $t = 0.22$ ms the speed of 20 m/s.

The residual speed of 20 m/s results to be 2.3% of the initial bullet velocity, so the numerical model is validated as it predicts a complete stop of the bullet inside the target and does not cause any rear pullout fragments phenomena of composite material as measured in the tests.

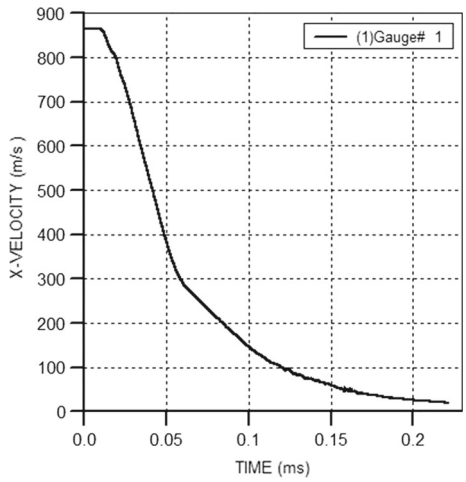

Fig. 25 Projectile velocity diagram

From Fig. 26, it is possible to evaluate the maximum deflection of the rear package and the diameter extension of the damaged area. The damage in the simulations is the maximum dynamic extension due to the high-velocity impact. Finally, it can be stated that the choice of increasing by 10% the fibers layers thickness is correct for obtaining results in agreement with the experimental tests already carried out. The numerical three-dimensional images allow a first qualitative comparison with the experimental tests images (see Fig. 27 in comparison to Figs. 11 and 13).

6.3 Numerical and experimental results comparison

Particular attention was paid to the maximum value of bulge deflection, as very significant to assess the rear damage produced by the threat. During ballistic tests, authors managed to evaluate the static damage due to the impact, the maximum value of the rear bulge after impact, and the dynamic damage in terms of maximum deflection in the transient dynamic phase using modeling clay. From the three-dimensional scans carried out on composite panels, the maximum value of the static deflection of each panel and the rear damage extension, specifically its maximum size, was assessed. These values were then compared to those obtained experimentally through destructive analysis in which the panels were analyzed in order to understand the damage mechanisms of each materials and the real damage dimensions due to the bullet impact. In Fig. 28, the three-dimensional scanning of the rear face of the composite panel and the perpendicular sections to the impact plane

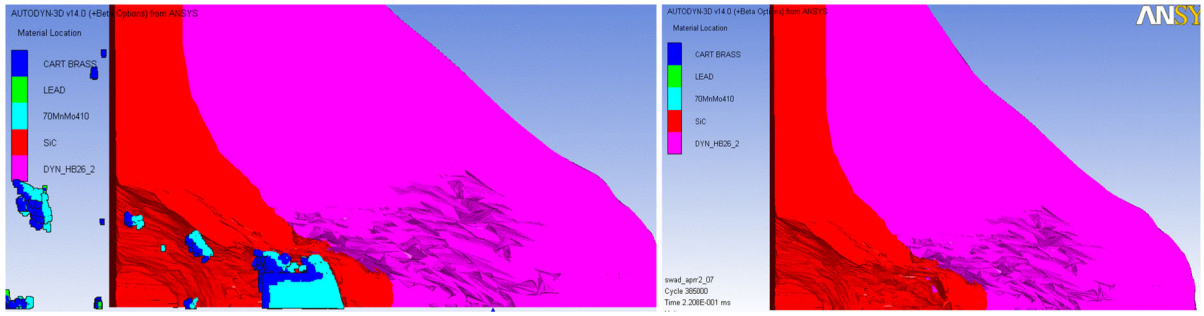

Fig. 26 Zooming on the point of impact

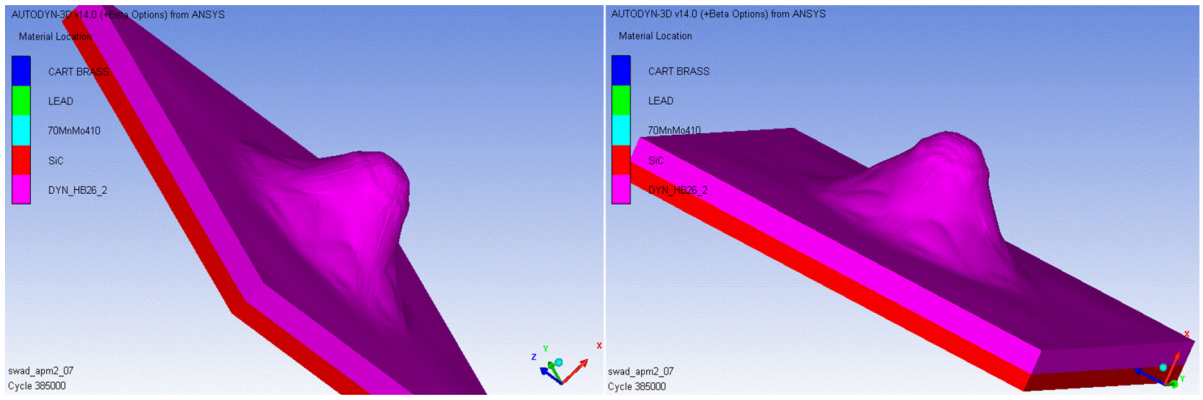

Fig. 27 Tri-dimensional simulated damaged area

are shown. On both images, the areas that present rear deflection values greater than 1 mm and the maximum values of the deflection measured at the impact point are highlighted. These values are significantly lower than those measured after the tests on the clay. Indeed, measured values do not exceed about 10–12 mm for all measured specimens while during the tests they deform much more at impact instant and then return in a final static deformed configuration.

The values for the three impacts on the specimens in term of maximum rear bulging, damage extension on the front of the fibers package and rear deflection area extension measured directly on the back-packing are summarized in Table 9 in normalized format.

Then, the numerical and experimental results are compared and commented as follows:

- Bulging: The maximum bulging value measured in the simulation turns out to be considerably greater than the static value measured after the tests. This discrepancy occurs because of the simulation time: The numerical simulation was stopped after 0.2 ms after the impact contact, i.e., during the dynamic transient phase of the penetration. The numerical bulging is therefore more in agreement with the real dynamic deflection measured on the clay. Namely, the clay average deflection measured a rather large penetration in the rear armor plate, about three times the static one. The numerical damage seems to be slightly higher than this value because of the back-clay layer absence in the simulation, certainly affecting the total panel deformation. To obtain comparable values, a longer numerical simulation, at least of a few milliseconds, is needed. This would imply more computational time to run a single simulation and, consequently, more computational power.
- Penetration damage defines the fibers rupture dimensions due to the impact in the front part of the armor panel. These numerical values are in good agreement with the experimental penetration values measured on the panels: the average experimental results are to be in the order of a few millimeters, which differ by 2.4% from the value determined in the numerical simulation. Therefore, the numerical bullet hole in the fiber layer seems to reproduce

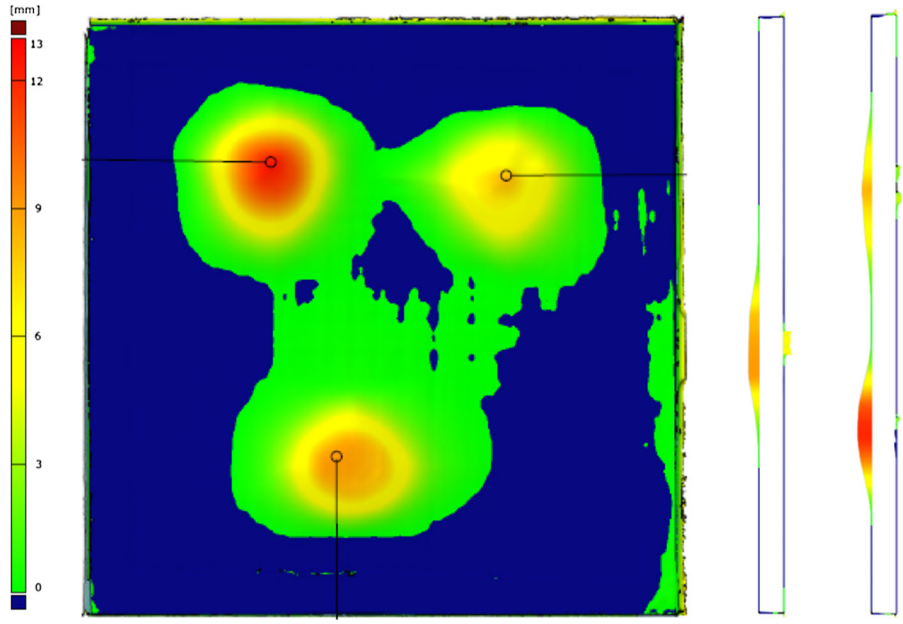

Fig. 28 Tri-dimensional scan of a panel

correctly the real penetration size of the projectile inside the composite target.

- Bulge propagation: The average extension of the rear bulging measured during the nondestructive test is of the order of 10–15 cm, less than 1% from the simulation result.
- Bullet penetration in the numerical model results to be 35% higher than the average penetration measured experimentally on the impact panels. However, the measurements are quite difficult to perform even during destructive test. Considering the difficulties to define the real damage and the uncertainty affecting the real numerical penetration values, this comparison can be considered as a good indication, but it does not represent a fully satisfactory information.

In general, the obtained numerical simulation results are satisfactory to define the complete stop of the bullet into the target and the obtained model can be used to optimize the layer thicknesses of the armor. Moreover, the obtained results also confirm a good degree of accuracy in the damage extension description for both the front and rear parts of the panel.

7 Conclusions

This work presents the development and validation of a numerical model for the simulation of high-velocity impact on advanced composite armor systems. Combining both mesh and meshless approaches, a highly refined numerical model was developed in the ANSYS-Autodyn® environment. An armor system made up by a first layer of SiC ceramic glued onto a back-packing made of UHWMPE laminate, was considered. Due to the lack of experimental and numerical results in the literature concerning this impact typology, a parallel experimental campaign was conducted in order to validate the numerical results: Three rectangular add-on panels were built, aimed at providing the fourth protection level (named Armor-Piercing Rifle) as defined by the NIJ Standard 0108.01 [22]. Namely, the level of threat considered is a 30-06 M2 Armour Piercing (AP) bullet.

On each panel, three M2 bullets were fired in points marked in correspondence of the SiC tiles. Once completed the experimental tests, nondestructive and destructive analyses were carried out on the panels, aimed at obtaining the characterization of the different types of damage and fractures due to the impact into ceramic material and into back-packing. These analyses also allowed displaying and defining the actual mechanism of penetration of the projectile inside the composite material.

In conclusion, the comparison reveals a good agreement between experimental and computational results in terms of ballistic properties, deformations, fragmen-

tation and fracture of the ballistic armor system. Such experimental/numerical comparison allows validating the numerical strategy adopted by the authors.

Acknowledgements The work has been partially funded by the Research Grant DPU12UNIGE82/6100 of Regione Liguria, Italy (Fondo Sociale Europeo Regione Liguria 2007–2013 Asse IV "Capitale Umano" ob.specifico I/6).

References

1. Anderson Jr., C.E., Cox, P.A., Johnson, G.R., Maudlin, P.J.: A constitutive formulation for anisotropic materials suitable for wave propagation computer programs–II. Comput. Mech. **15**(3), 201–223 (1994)
2. ANSYS: Ansys Help System. ANSYS, s.l. (2010)
3. Clegg, R., Hayhurst, C., Livingstone, I., Francis, N.: The Application of SPH Techniques in Autodyn-2D to Ballistic Impact Problems. San Francisco/CA, USA, s.n. (1996)
4. Cunniff, P.: Dimensionless Parameters for Optimization of Textile-based Body Armor Systems, pp. 1301–10. San Antonio Texas, Technomic Publishing, Lancaster, PA (1999)
5. Fallah, A.S., Micallef, K., Langdon, G.S., Lee, W.C., Curtis, P.T., Louca, L.A.: Dynamic response of Dyneema® HB26 plates to localised blast loading. Int. J. Impact Eng. **73**, 91–100 (2014)
6. Fecko, D., Lyle, D., Xavier, G.: Composite armor solution for STANAG 4569 ballistic protection levels. In: SAMPE Europe, Paper SE 05-34, Paris, France (2005)
7. Flores-Johnson, E.A., Saleh, M., Edwards, L.: Ballistic performance of multi-layered metallic plates impacted by a 7.62-mm APM2 projectile. Int. J. Impact Eng. **38**(12), 1022–1032 (2011)
8. Forrestal, M.J., Børvik, T., Warren, T.L.: Perforation of 7075–T651 aluminum armor plates with 7.62 mm APM2 bullets. Exp. Mech. **50**(8), 1245–1251 (2010)
9. Frissen, R.: Modeling the Ballistic Impact Behaviour of Polyethylene-fibre-reinforced Composites. Eindhoven University of Technology, Eindhoven (1996)
10. Grujicic, M., Arakere, G., He, T., Bell, W.C., Cheeseman, B.A., Yen, C.-F., Scott, B.: A ballistic material model for cross-plied unidirectional ultra-high molecular-weight polyethylene fiber-reinforced armor-grade composites. Mater. Sci. Eng. A **498**(1–2), 231–241 (2008)
11. Grujicic, M., Bell, W.C., Thompson, L.L., Koudela, K.L., Cheeseman, B.A.: Ballistic-protection performance of carbon-nanotube-doped poly-vinyl-ester-epoxy matrix composite armor reinforced with E-glass fiber mats. Mater. Sci. Eng. A **479**(1–2), 10–22 (2008)
12. Grujicic, M., Pandurangan, B., Koudela, K.L., Cheeseman, B.A.: A computational analysis of the ballistic performance of light-weight hybrid composite armors. Appl. Surface Sci. **253**(2), 730–745 (2006)
13. Hayhurst, C.J., Hiermaier, S.J., Clegg, R.A., Riedel, W., Lambert, M.: Development of material models for Nextel and Kevlar-epoxy for high pressures and strain rates. Int. J. Impact Eng. **23**(1 PART I), 365–376 (1999)
14. Hogg, P.: Composites for Ballistic Applications. Queen Mary, University of London, London (2003)
15. Holmquist, T.J., Johnson, G.R.: Characterization and evaluation of silicon carbide for high-velocity impact. J. Appl. Phys. **97**(9), 093502 (2005)
16. Iannucci, L., Pope, D., Dalzell, M.: A Constitutive Model for Dyneema UD Composites, p. 10. The British Composites Society, Edinburgh (2009)
17. Johnson, G.R., Cook, W.H.: A constitutive model and data for metals subjected to large strains, high strain rates, and high temperatures. In: Proceedings 7th International Symposium on Ballistics, The Hague, 19–21 April 1983, pp. 541–547 (1983)
18. Karthikeyan, K., Russell, B.P., Fleck, N.A., Wadley, H.N.G., Deshpande, V.S.: The effect of shear strength on the ballistic response of laminated composite plates. Eur. J. Mech. A Solids **42**, 35–53 (2013)
19. Lässig, T., Riedel, W., Heisserer, U., Van der Werff, H., May, M., Hiermaier, S.: Numerical sensitivity studies of a UHMWPE composite for ballistic protection. WIT Trans. Built Environ. **141**, 371–381 (2014)
20. Lässig, T., Nguyen, L., May, M., Riedel, W., Heisserer, U., Van Der Werff, H., Hiermaier, S.: A non-linear orthotropic hydrocode model for ultra-high molecular weight polyethylene in impact simulations. Int. J. Impact Eng. **75**, 110–122 (2015)
21. Lim, C.T., Shim, V.P.W., Ng, Y.H.: Finite-element modeling of the ballistic impact of fabric armor. Int. J. Impact Eng. **28**(1), 13–31 (2003)
22. National Institute of Justice: Ballistic Resistant Protective Materials—NIJ Standard 0108.01. U.S. Department of Justice, Washington, DC (1985)
23. Nato, S.a: STANAG 4569 Land (Edition 1)—Protection Levels for Occupants of Logistic and Light Armoured Vehicles. NATO, Brussels (2004)
24. O'Masta, M.R., Deshpande, V.S., Wadley, H.N.G.: Mechanisms of projectile penetration in Dyneema® encapsulated aluminum structures. Int. J. Impact Eng. **74**, 16–35 (2014)
25. Ramadhan, A.A., Abu Talib, A.R., Mohd Rafie, A.S., Zahari, R.: High velocity impact response of Kevlar-29/epoxy and 6061-T6 aluminum laminated panels. Mater. Des. **43**, 307–321 (2013)
26. Russell, B.P., Karthikeyan, K., Deshpande, V.S., Fleck, N.A.: The high strain rate response of ultra high molecular-weight polyethylene: from fibre to laminate. Int. J. Impact Eng. **60**, 1–9 (2013)
27. Sabadin, G., Bassano, A., Rizzo, C., Gaiotti, M.: Modellazione e simulazione d'impatti ad alta velocità. Report no: 13GSA02. s.l.: OTO Melara (2013)
28. Sabadin, G., Gaiotti, M., Rizzo, C., Bassano, A.: Optimization of ballistic properties of an advanced composite armor system: analysis and validation of numerical models subject to High Velocity Impacts. In: Maritime Technology ad Engineering, pp. 463–475. C. Guedes Soares, T.A. Santos, Lisbon (2014)
29. Steinberg, D.: Equation of State and Strength Properties of Selected Materials. Lawrence Livermore National Laboratories Report, s.l. (1991)